Spin-3/2 nucleon and Δ baryons in lattice QCD

J. M. Zanotti, D. B. Leinweber, A. G. Williams, and J. B. Zhang

Department of Physics and Mathematical Physics, and Special Research Centre for the Subatomic Structure of Matter,
University of Adelaide, Adelaide 5005, Australia

W. Melnitchouk

Jefferson Lab, 12000 Jefferson Avenue, Newport News, Virginia 23606, USA

S. Choe

Korea Advanced Institute of Science and Technology, 373-1, Guseong-dong, Yuseong-gu, Daejon 305-701, Republic of Korea

(CSSM Lattice Collaboration)

We present the first results for masses of spin-$\frac{3}{2}$ N and Δ baryons in lattice QCD using fat-link irrelevant clover fermions. Spin-$\frac{3}{2}$ interpolating fields, providing overlap with both spin-$\frac{3}{2}$ and spin-$\frac{1}{2}$ states, are considered. In the isospin-$\frac{1}{2}$ sector we observe, after appropriate spin and parity projection, a strong signal for the $J^P = \frac{3}{2}^-$ state together with a weak but discernible signal for the $\frac{3}{2}^+$ state with a mass splitting near that observed experimentally. We also find good agreement between the $\frac{1}{2}^{\pm}$ masses and earlier nucleon mass simulations with the standard spin-$\frac{1}{2}$ interpolating field. For the isospin-$\frac{3}{2}$ Δ states, clear mass splittings are observed between the various $\frac{1}{2}^{\pm}$ and $\frac{3}{2}^{\pm}$ channels, with the calculated level orderings in good agreement with those observed empirically.

I. INTRODUCTION

The level orderings in the baryon spectrum and mass splittings between excited baryon multiplets provide important clues to the underlying dynamics governing interquark forces and the relevant effective degrees of freedom at low energy [1]. Considerable insight into these and other problems of spectroscopy has been gained from QCD-inspired phenomenological models; however, many fundamental questions about the origins of the empirical spectrum remain controversial [2].

The resolution of some of these issues may only be possible with the help of calculations of the spectrum in lattice QCD—currently the only first-principles method able to determine hadron properties directly from the fundamental quark and gluon theory. Recent advances in computational capabilities and more efficient algorithms have enabled the first dedicated lattice QCD simulations of the excited states of the nucleon to be undertaken [3–10]. Lattice studies of excited hadrons are possible because at the current unphysically large quark masses and finite volumes used in the simulations, most excited states are stable. Contact with experiment can be made via extrapolations incorporating the nonanalytic behavior of chiral effective field theory [11]. These studies are timely as they complement the first results from the high precision measurements of the N^* spectrum at Jefferson Lab [12].

In a recent paper [9] we presented the first results for the excited nucleon and spin-$\frac{1}{2}$ hyperon spectra using the fat-link irrelevant clover (FLIC) quark action [13] with an $O(a^2)$-improved gluon action. The FLIC action minimizes the effect of renormalization of action improvement terms and displays excellent scaling properties [13]. Clear mass splittings are observed for $J^P = \frac{1}{2}^+$ and $\frac{1}{2}^-$ states, as well as

evidence for the sensitivity to hyperfine splittings of odd-parity states for different interpolating fields used. On the other hand, no evidence is seen for overlap of three-quark interpolating fields with the Roper-like resonances or the lowest-lying odd-parity SU(3) singlet state, the $\Lambda(1405)$. In this paper we extend the analysis of Ref. [9] to the spin-$\frac{3}{2}$ sector, and present first results using the FLIC action, in both the isospin-$\frac{1}{2}$ and -$\frac{3}{2}$ channels.

Mass splittings between states within SU(3) quark-model multiplets provide another important motivation for studying higher spin baryons. Understanding the mass splitting between the $N\frac{1}{2}^-(1535)$ and $N\frac{3}{2}^-(1520)$, for instance, or between the $\Delta\frac{1}{2}^-(1620)$ and $\Delta\frac{3}{2}^-(1700)$, can help identify the important mechanisms associated with the hyperfine interactions, or shed light on the spin-orbit force, which has been a central mystery in spectroscopy [14]. In valence quark models, the degeneracy between the $N\frac{1}{2}^-$ and $N\frac{3}{2}^-$ can be broken by a tensor force associated with mixing between the N^2 and N^4 representations of SU(3) [2], although this generally leaves the $N\frac{3}{2}^-$ at a higher energy than the $N\frac{1}{2}^-$. On the other hand, a spin-orbit force is necessary to split the $\Delta\frac{3}{2}^-$ and $\Delta\frac{1}{2}^-$ states. In the Goldstone boson exchange model [15], both of these pairs of states are degenerate. Model-independent analyses in the large N_c limit have found that these mass splittings receive important contributions from operators that do not have a simple quark model interpretation [16], such as those simultaneously coupling spin, isospin and orbital angular momentum. Of course, the coefficients of the various operators in such an analysis must be determined phenomenologically and guidance from lattice QCD is essential.

Our lattice simulations are performed on the Orion com-

puter cluster dedicated to lattice QCD at the Center for the Subatomic Structure of Matter (CSSM), University of Adelaide. In the isospin-$\frac{3}{2}$ sector, after applying suitable parity and spin projections, we present the first results for the $\Delta\frac{1}{2}^+$ and $\Delta\frac{1}{2}^-$ states, as well as the $\Delta\frac{3}{2}^-$. Our results for the $\Delta\frac{3}{2}^+$ are also in good agreement with earlier simulations [17]. A significant advance of this work is the observation of a discernible signal for the $\Delta\frac{1}{2}^\pm$ state, which yielded a weak signal in earlier simulations [6]. The lowest excitation of the ground state, namely the $\Delta\frac{1}{2}^-$, is found to have a mass ~ 350–400 MeV above the $\Delta\frac{3}{2}^+$, with the $\Delta\frac{3}{2}^-$ slightly heavier. The $\Delta\frac{1}{2}^+$ state is found to lie ~ 100–200 MeV above these, although the signal becomes weak at smaller quark masses. This level ordering is consistent with that observed in the empirical mass spectrum.

In the spin-$\frac{3}{2}$ nucleon sector, there is good agreement for the spin-projected $\frac{1}{2}^+$ and $\frac{1}{2}^-$ states with earlier nucleon mass calculations [9] using the standard spin-$\frac{1}{2}$ nucleon interpolating field. Furthermore, we find a good signal for the $N\frac{3}{2}^\pm$ states, with a mass difference of ~ 300 MeV between the spin-$\frac{3}{2}$ parity partners. The $N\frac{1}{2}^-$ and $N\frac{3}{2}^-$ states are approximately degenerate as observed experimentally.

In Sec. II we outline the basic elements of formulating spin-$\frac{3}{2}$ baryons on the lattice, including the choice of interpolating fields and projection operators. A brief preliminary report of states using the formalism developed and presented here appeared in Ref. [18]. These results also supersede preliminary results reported in Refs. [19,20]. In Sec. III, our results using the FLIC action on a large lattice volume at a fine lattice spacing represent the first quantitative analysis of these states. The conclusion and remarks about future work are contained in Sec. IV.

II. SPIN-3/2 BARYONS ON THE LATTICE

A. Spin-3/2 interpolating fields and two-point functions

In this section the essential elements for a lattice calculation of spin-$\frac{3}{2}$ baryon properties are presented. The mass of a spin-$\frac{3}{2}$ baryon on the lattice is obtained from the two-point correlation function $G_{\mu\nu}$ [17],

$$G_{\mu\nu}(t,\vec{p};\Gamma) = \mathrm{tr}_{\mathrm{sp}}\{\Gamma \mathcal{G}_{\mu\nu}(t,\vec{p})\}, \tag{1}$$

where

$$\mathcal{G}_{\mu\nu}^{\alpha\beta}(t,\vec{p}) = \sum_{\vec{x}} e^{-i\vec{p}\cdot\vec{x}}\langle 0|T(\chi_\mu^\alpha(x)\bar{\chi}_\nu^\beta(0))|0\rangle, \tag{2}$$

where χ_μ^α is a spin-$\frac{3}{2}$ interpolating field, Γ is a matrix in Dirac space with α,β Dirac indices, and μ,ν Lorentz indices.

In this analysis we consider the following interpolating field operator for the isospin-$\frac{1}{2}$, spin-$\frac{3}{2}$, positive parity (charge $+1$) state [21]:

$$\chi_\mu^N = \epsilon^{abc}(u^{Ta}(x)C\gamma_5\gamma^\nu d^b(x))\left(g_{\mu\nu} - \frac{1}{4}\gamma_\mu\gamma_\nu\right)\gamma_5 u^c(x). \tag{3}$$

All discussions of interpolating fields are carried out using the Dirac representation of the γ matricies. This exact isospin-$\frac{1}{2}$ interpolating field has overlap with both spin-$\frac{3}{2}$ and spin-$\frac{1}{2}$ states and with states of both parities. The resulting correlation function will thus require both spin and parity projection. The quark field operators u and d act at Euclidean space-time point x, C is the charge conjugation matrix, a,b and c are color labels, and the superscript T denotes the transpose. The charge neutral interpolating field is obtained by interchanging $u \leftrightarrow d$. This interpolating field transforms as a Rarita-Schwinger operator under parity transformations. That is, if the quark field operators transform as

$$\mathcal{P}u(x)\mathcal{P}^\dagger = +\gamma_0 u(\tilde{x}),$$

where $\tilde{x} = (x_0, -\vec{x})$, and similarly for $d(x)$, then

$$\mathcal{P}\chi_\mu^N(x)\mathcal{P}^\dagger = +\gamma_0 \chi_\mu^N(\tilde{x}),$$

and similarly for the Rarita-Schwinger operator

$$\mathcal{P}u_\mu(x)\mathcal{P}^\dagger = +\gamma_0 u_\mu(\tilde{x}), \tag{4}$$

which will be discussed later.

The computational cost of evaluating each of the Lorentz combinations in Eq. (3) is relatively high—about 100 times that for the ground state nucleon [4]. Consequently, in order to maximize statistics in our analysis we consider only the leading term proportional to $g_{\mu\nu}$ in the interpolating field,

$$\chi_\mu^N \to \epsilon^{abc}(u^{Ta}(x)C\gamma_5\gamma_\mu d^b(x))\gamma_5 u^c(x). \tag{5}$$

This is sufficient since we will in either case need to perform a spin-$\frac{3}{2}$ projection.

In order to show that the interpolating field defined in Eq. (5) has isospin-$\frac{1}{2}$, we first consider the standard proton interpolating field,

$$\chi^p = \epsilon^{abc}(u^{Ta}C\gamma_5 d^b)u^c, \tag{6}$$

which we know to have isospin-$\frac{1}{2}$. Applying the isospin raising operator I^+ on χ^p, one finds

$$\begin{aligned}
I^+\chi^p &= \epsilon^{abc}(u^{Ta}C\gamma_5 u^b)u^c \\
&= \epsilon^{abc}(u^{Ta}C\gamma_5 u^b)^T u^c \\
&= -\epsilon^{abc}(u^{Ta}C\gamma_5 u^b)u^c \\
&= 0.
\end{aligned}$$

Similarly, for the interpolating field defined in Eq. (5), one has

$$\begin{aligned}
I^+\chi_\mu^N &= \epsilon^{abc}(u^{Ta}C\gamma_5\gamma_\mu u^b)\gamma_5 u^c \\
&= \epsilon^{abc}(u^{Ta}C\gamma_5\gamma_\mu u^b)^T \gamma_5 u^c \\
&= -\epsilon^{abc}(u^{Ta}C\gamma_5\gamma_\mu u^b)\gamma_5 u^c \\
&= 0,
\end{aligned}$$

where we have used the representation independent identities $C\gamma_\mu C^{-1}=-\gamma_\mu^T$, $C\gamma_5 C^{-1}=\gamma_5^T$ and the identities which hold in the Dirac representation $C^T=C^\dagger=C^{-1}=-C$ with $C=i\gamma_2\gamma_0$ and $\gamma_5^T=\gamma_5$.

We note that $\bar{\chi}_\mu^N$ corresponding to χ_μ^N in Eq. (5) is

$$\bar{\chi}_\mu^N=\epsilon^{abc}\bar{u}^a\gamma_5(\bar{d}^b\gamma_\mu\gamma_5 C\bar{u}^{cT}), \tag{7}$$

so that

$$\chi_\mu^N\bar{\chi}_\nu^N=\epsilon^{abc}\epsilon^{a'b'c'}(u_\alpha^{Ta}[C\gamma_5\gamma_\mu]_{\alpha\beta}d_\beta^b)\gamma_5 u_\gamma^c\bar{u}_{\gamma'}^{c'}\gamma_5$$
$$\times(\bar{d}_{\beta'}^{b'}[\gamma_\nu\gamma_5 C]_{\beta'\alpha'}\bar{u}_{\alpha'}^{Ta'})$$
$$\rightarrow\gamma_5 S_u\gamma_5\text{Tr}[\gamma_5 S_u\gamma_5(C\gamma_\mu S_d\gamma_\nu C)^T]$$
$$+\gamma_5 S_u\gamma_5(C\gamma_\mu S_d\gamma_\nu C)^T\gamma_5 S_u\gamma_5, \tag{8}$$

where the last two lines are the result achieved after doing the Grassman integration over the quark fields with the quark fields being replaced by all possible pairwise contractions.

In deriving the Δ interpolating fields, it is simplest to begin with the state containing only valence u quarks, namely the Δ^{++}. The interpolating field for the Δ^{++} resonance is given by [21],

$$\chi_\mu^{\Delta^{++}}(x)=\epsilon^{abc}(u^{Ta}(x)C\gamma_\mu u^b(x))u^c(x), \tag{9}$$

which also transforms as a pseudovector under parity. The interpolating field for a Δ^+ state can be similarly constructed [17],

$$\chi_\mu^{\Delta^+}(x)=\frac{1}{\sqrt{3}}\epsilon^{abc}[2(u^{Ta}(x)C\gamma_\mu d^b(x))u^c(x)$$
$$+(u^{Ta}(x)C\gamma_\mu u^b(x))d^c(x)]. \tag{10}$$

Interpolating fields for other decuplet baryons are obtained by appropriate substitutions of u, $d\rightarrow u$, d or s fields.

To project a pure spin-$\frac{3}{2}$ state from the correlation function $G_{\mu\nu}$, one needs to use an appropriate spin-$\frac{3}{2}$ projection operator [22],

$$P_{\mu\nu}^{3/2}(p)=g_{\mu\nu}-\frac{1}{3}\gamma_\mu\gamma_\nu-\frac{1}{3p^2}(\gamma\cdot p\,\gamma_\mu p_\nu+p_\mu\gamma_\nu\gamma\cdot p). \tag{11}$$

The corresponding spin-$\frac{1}{2}$ state can be projected by applying the projection operator

$$P_{\mu\nu}^{1/2}=g_{\mu\nu}-P_{\mu\nu}^{3/2}. \tag{12}$$

To use this operator and retain all Lorentz components, one must calculate the full 4×4 matrix in Dirac and Lorentz space. However, to extract a mass, only one pair of Lorentz indices is needed, reducing the amount of calculations required by a factor of four. We calculate the third row of the Lorentz matrix and use the projection

$$G_{33}^s=\sum_{\mu,\nu=1}^4 G_{3\mu}g^{\mu\nu}P_{\nu3}^s, \tag{13}$$

to extract the desired spin states, $s=\frac{1}{2}$ or $\frac{3}{2}$. Following spin projection, the resulting correlation function, G_{33}^s, still contains positive and negative parity states.

B. Baryon level

The interpolating field operators defined in Eqs. (3) and (5) have overlap with both spin-$\frac{3}{2}$ and spin-$\frac{1}{2}$ states with positive and negative parity. The field χ_μ transforms as a pseudovector under parity, as does the Rarita-Schwinger spinor, u_μ. Thus the overlap of χ_μ with baryons can be expressed as

$$\langle 0|\chi_\mu|N^{3/2^+}(p,s)\rangle=\lambda_{3/2^+}\sqrt{\frac{M_{3/2^+}}{E_{3/2^+}}}u_\mu(p,s), \tag{14a}$$

$$\langle 0|\chi_\mu|N^{3/2^-}(p,s)\rangle=\lambda_{3/2^-}\sqrt{\frac{M_{3/2^-}}{E_{3/2^-}}}\gamma_5 u_\mu(p,s), \tag{14b}$$

$$\langle 0|\chi_\mu|N^{1/2^+}(p,s)\rangle=(\alpha_{1/2^+}p_\mu+\beta_{1/2^+}\gamma_\mu)$$
$$\times\sqrt{\frac{M_{1/2^+}}{E_{1/2^+}}}\gamma_5 u(p,s), \tag{14c}$$

$$\langle 0|\chi_\mu|N^{1/2^-}(p,s)\rangle=(\alpha_{1/2^-}p_\mu+\beta_{1/2^-}\gamma_\mu)$$
$$\times\sqrt{\frac{M_{1/2^-}}{E_{1/2^-}}}u(p,s), \tag{14d}$$

where the factors $\lambda_B,\alpha_B,\beta_B$ denote the coupling strengths of the interpolating field χ_μ to the baryon B and $E_B=\sqrt{\vec{p}^2+M_B^2}$ is the energy. For the expressions in Eqs. (14c) and (14d), we note that the spatial components of momentum p_i transform as a vector under parity and commute with γ_0, whereas the γ_i do not change sign under parity but anticommute with γ_0. Hence the right-hand side of Eq. (14c) also transforms as a pseudovector under parity in accord with χ_μ.

Similar expressions can also be written for $\bar{\chi}_\mu$,

$$\langle N^{3/2^+}(p,s)|\bar{\chi}_\mu|0\rangle=\lambda_{3/2^+}^*\sqrt{\frac{M_{3/2^+}}{E_{3/2^+}}}\bar{u}_\mu(p,s), \tag{15a}$$

$$\langle N^{3/2^-}(p,s)|\bar{\chi}_\mu|0\rangle=-\lambda_{3/2^-}^*\sqrt{\frac{M_{3/2^-}}{E_{3/2^-}}}\bar{u}_\mu(p,s)\gamma_5, \tag{15b}$$

$$\langle N^{1/2^+}(p,s)|\bar{\chi}_\mu|0\rangle=-\sqrt{\frac{M_{1/2^+}}{E_{1/2^+}}}\bar{u}(p,s)$$
$$\times\gamma_5(\alpha_{1/2^+}^*p_\mu+\beta_{1/2^+}^*\gamma_\mu), \tag{15c}$$

$$\langle N^{1/2-}(p,s)|\bar{\chi}_\mu|0\rangle = \sqrt{\frac{M_{1/2^-}}{E_{1/2^-}}}\bar{u}(p,s)$$
$$\times(\alpha^*_{1/2^-}p_\mu + \beta^*_{1/2^-}\gamma_\mu). \qquad (15d)$$

Note that we are assuming identical sinks and sources in these equations. In our calculations we use a smeared source and a point sink in which case λ^*, α^* and β^* are no longer complex conjugates of λ, α and β and are instead replaced by $\bar{\lambda}$, $\bar{\alpha}$ and $\bar{\beta}$.

We are now in a position to find the form of Eq. (2) after we insert a complete set of intermediate states $\{|B(p,s)\rangle\}$. The contribution to Eq. (2) from each intermediate state considered is given by

$$\langle 0|\chi_\mu|N^{3/2+}(p,s)\rangle\langle N^{3/2+}(p,s)|\bar{\chi}_\nu|0\rangle$$
$$= +\lambda_{3/2^+}\bar{\lambda}_{3/2^+}\frac{M_{3/2^+}}{E_{3/2^+}}u_\mu(p,s)\bar{u}_\nu(p,s)$$
$$= -\lambda_{3/2^+}\bar{\lambda}_{3/2^+}\frac{M_{3/2^+}}{E_{3/2^+}}\frac{(\gamma\cdot p+M_{3/2^+})}{2M_{3/2^+}}$$
$$\times\left\{g_{\mu\nu} - \frac{1}{3}\gamma_\mu\gamma_\nu - \frac{2p_\mu p_\nu}{3M^2_{3/2^+}} + \frac{p_\mu\gamma_\nu - p_\nu\gamma_\mu}{3M_{3/2^+}}\right\},$$

$$\langle 0|\chi_\mu|N^{3/2-}(p,s)\rangle\langle N^{3/2-}(p,s)|\bar{\chi}_\nu|0\rangle$$
$$= -\lambda_{3/2^-}\bar{\lambda}_{3/2^-}\frac{M_{3/2^-}}{E_{3/2^-}}\gamma_5 u_\mu(p,s)\bar{u}_\nu(p,s)\gamma_5$$
$$= -\lambda_{3/2^-}\bar{\lambda}_{3/2^-}\frac{M_{3/2^-}}{E_{3/2^-}}\frac{(\gamma\cdot p - M_{3/2^-})}{2M_{3/2^-}}$$
$$\times\left\{g_{\mu\nu} - \frac{1}{3}\gamma_\mu\gamma_\nu - \frac{2p_\mu p_\nu}{3M^2_{3/2^-}} - \frac{p_\mu\gamma_\nu - p_\nu\gamma_\mu}{3M_{3/2^-}}\right\},$$

$$\langle 0|\chi_\mu|N^{1/2+}(p,s)\rangle\langle N^{1/2+}(p,s)|\bar{\chi}_\nu|0\rangle$$
$$= -\frac{M_{1/2^+}}{E_{1/2^+}}(\alpha_{1/2^+}p_\mu + \beta_{1/2^+}\gamma_\mu)\gamma_5\frac{\gamma\cdot p+M_{1/2^+}}{2M_{1/2^+}}$$
$$\times\gamma_5(\bar{\alpha}_{1/2^+}p_\nu + \bar{\beta}_{1/2^+}\gamma_\nu),$$

$$\langle 0|\chi_\mu|N^{1/2-}(p,s)\rangle\langle N^{1/2-}(p,s)|\bar{\chi}_\nu|0\rangle$$
$$= \frac{M_{1/2^-}}{E_{-/2^+}}(\alpha_{1/2^-}p_\mu + \beta_{1/2^-}\gamma_\mu)\frac{\gamma\cdot p+M_{1/2^-}}{2M_{1/2^-}}$$
$$\times(\bar{\alpha}_{1/2^-}p_\nu + \bar{\beta}_{1/2^-}\gamma_\nu).$$

To reduce computational expense, we consider the specific case when $\mu=\nu=3$ and in order to extract masses we require $\vec{p}=(0,0,0)$. In this case we have the simple expressions

$$\langle 0|\chi_3|N^{3/2+}(p,s)\rangle\langle N^{3/2+}(p,s)|\bar{\chi}_3|0\rangle$$
$$= \lambda_{3/2^+}\bar{\lambda}_{3/2^+}\frac{2}{3}\left(\frac{\gamma_0 M_{3/2^+}+M_{3/2^+}}{2M_{3/2^+}}\right), \qquad (16a)$$

$$\langle 0|\chi_3|N^{3/2-}(p,s)\rangle\langle N^{3/2-}(p,s)|\bar{\chi}_3|0\rangle$$
$$= \lambda_{3/2^-}\bar{\lambda}_{3/2^-}\frac{2}{3}\left(\frac{\gamma_0 M_{3/2^-}-M_{3/2^-}}{2M_{3/2^-}}\right), \qquad (16b)$$

$$\langle 0|\chi_3|N^{1/2+}(p,s)\rangle\langle N^{1/2+}(p,s)|\bar{\chi}_3|0\rangle$$
$$= -\beta_{1/2^+}\bar{\beta}_{1/2^+}\gamma_3\gamma_5\frac{\gamma_0 M_{1/2^+}+M_{1/2^+}}{2M_{1/2^+}}\gamma_5\gamma_3$$
$$= +\beta_{1/2^+}\bar{\beta}_{1/2^+}\frac{\gamma_0 M_{1/2^+}+M_{1/2^+}}{2M_{1/2^+}}, \qquad (16c)$$

$$\langle 0|\chi_3|N^{1/2-}(p,s)\rangle\langle N^{1/2-}(p,s)|\bar{\chi}_3|0\rangle$$
$$= \beta_{1/2^-}\bar{\beta}_{1/2^-}\gamma_3\frac{\gamma_0 M_{1/2^-}+M_{1/2^-}}{2M_{1/2^-}}\gamma_3$$
$$= +\beta_{1/2^-}\bar{\beta}_{1/2^-}\frac{\gamma_0 M_{1/2^-}-M_{1/2^-}}{2M_{1/2^-}}. \qquad (16d)$$

Therefore, in an analogous procedure to that used in Ref. [9], where a fixed boundary condition is used in the time direction, positive and negative parity states are obtained by taking the trace of the spin-projected correlation function, G^s_{33}, in Eq. (13) with the operator $\Gamma = \Gamma_\pm$,

$$G^{s\pm}_{33} = \mathrm{tr}_{sp}\{\Gamma^\pm G^s_{33}\}, \qquad (17)$$

where

$$\Gamma_\pm = \frac{1}{2}(1\pm\gamma_4). \qquad (18)$$

The positive parity states propagate in the (1,1) and (2,2) elements of the Dirac matrix, while negative parity states propagate in the (3,3) and (4,4) elements for both spin-$\frac{1}{2}$ and spin-$\frac{3}{2}$ projected states. A similar treatment has been carried out for the Δ interpolating fields but is not reproduced here for brevity.

We use an improved unbiased estimator obtained by summing both U and U^* configurations which occur with equal weight. From the discussion given in Sec. V A of Ref. [9], $G^{s\pm}_{\mu\nu}$ is purely real if μ and ν are both spatial indicies or both temporal indicies, otherwise $G^{s\pm}_{\mu\nu}$ is purely imaginary.

III. RESULTS

The analysis is based on a sample of 392 configurations. For the gauge fields, a mean-field improved plaquette plus rectangle action is used. The simulations are performed on a $16^3\times32$ lattice at $\beta=4.60$, which corresponds to a lattice

spacing of $a = 0.122(2)$ fm set by a string tension analysis incorporating the lattice Coulomb potential [23] with $\sqrt{\sigma} = 440$ MeV. For the quark fields, a fat-link irrelevant clover (FLIC) [13] action is implemented. The use of fat links [24] in the irrelevant operators of the fermion action removes the need to fine tune the clover coefficient to remove $\mathcal{O}(a)$ artifacts. The use of fat links also allows us to employ a highly improved definition of $F_{\mu\nu}$ [13,25] leaving errors of $\mathcal{O}(a^6)$ and where errors of $\mathcal{O}(g^2)$ are suppressed via fat links. Mean-field improvement of the tree-level clover coefficient with fat links represents a small correction and proves to be adequate [13].

The fattening, or smearing of the lattice links with their nearest neighbors, reduces the problem of exceptional configurations, and minimizes the effect of renormalization on the action improvement terms. By smearing only the irrelevant, higher dimensional terms in the action, and leaving the relevant dimension-four operators untouched, we retain short distance quark and gluon interactions at the scale of the cutoff. Simulations are performed with $n = 4$ smearing sweeps and a smearing fraction $\alpha = 0.7$ [13].

A fixed boundary condition in the time direction is used for the fermions by setting $U_t(\vec{x}, N_t) = 0 \ \forall \ \vec{x}$ in the hopping terms of the fermion action, with periodic boundary conditions imposed in the spatial directions. Gauge-invariant Gaussian smearing [26] in the spatial dimensions is applied at the source to increase the overlap of the interpolating operators with the ground states. The source-smearing technique [26] starts with a point source,

$$\psi_{0\alpha}^a(\vec{x},t) = \delta^{ac}\delta_{\alpha\gamma}\delta_{\vec{x},\vec{x}_0}\delta_{t,t_0} \tag{19}$$

for source color c, Dirac γ, position $\vec{x}_0 = (1,1,1)$ and time $t_0 = 3$ and proceeds via the iterative scheme,

$$\psi_i(\vec{x},t) = \sum_{\vec{x}'} F(\vec{x},\vec{x}')\psi_{i-1}(\vec{x}',t),$$

where

$$F(\vec{x},\vec{x}') = \frac{1}{(1+\alpha)}\left(\delta_{\vec{x},\vec{x}'} + \frac{\alpha}{6}\sum_{\mu=1}^{3}[U_\mu(\vec{x},t)\delta_{\vec{x}',\vec{x}+\hat\mu}\right.$$

$$\left. + U_\mu^\dagger(\vec{x}-\hat\mu,t)\delta_{\vec{x}',\vec{x}-\hat\mu}]\right).$$

Repeating the procedure N times gives the resulting fermion source

$$\psi_N(\vec{x},t) = \sum_{\vec{x}'} F^N(\vec{x},\vec{x}')\psi_0(\vec{x}',t). \tag{20}$$

The parameters N and α govern the size and shape of the smearing function. We simulate with $N = 20$ and $\alpha = 6$. The propagator, S, is obtained from the smeared source by solving

$$M_{\alpha\beta}^{ab}S_{\beta\gamma}^{bc} = \psi_\alpha^a, \tag{21}$$

TABLE I. Masses of the π, $N^{\frac{1}{2}^\pm}$ and $N^{\frac{3}{2}^\pm}$ for several values of κ obtained from the spin-$\frac{3}{2}$ interpolating field, for the FLIC action with 4 sweeps of smearing at $\alpha = 0.7$. Here the value of κ_{cr} is $\kappa_{cr} = 0.1300$. A string tension analysis provides $a = 0.122(2)$ fm for $\sqrt{\sigma} = 440$ MeV.

κ	$m_\pi a$	$M_{N(1/2)+}a$	$M_{N(1/2)-}a$	$M_{N(3/2)+}a$	$M_{N(3/2)-}a$
0.1260	0.5767(11)	1.102(8)	1.412(13)	1.628(34)	1.410(16)
0.1266	0.5305(12)	1.043(9)	1.369(14)	1.577(38)	1.365(19)
0.1273	0.4712(15)	0.970(13)	1.317(17)	1.510(44)	1.312(24)
0.1279	0.4164(15)	0.905(18)	1.271(21)	1.440(53)	1.264(32)
0.1286	0.3421(18)	0.829(32)	1.220(31)	1.329(74)	1.206(49)

for each color, Dirac source c, γ, respectively, of Eq. (19) via the bistabilised conjugate gradient algorithm [27].

In the analysis we use five values of κ, as indicated in Table I. Extrapolation to $m_\pi^2 = 0$ gives $\kappa_{cr} = 0.1300$. Figure 1 shows the effective mass plot for the $N^{\frac{3}{2}^-}$ state for the five κ values used as a function of Euclidean time obtained after performing spin and parity projections on the correlation functions calculated using the interpolating field in Eq. (5). We find a good signal for this state up until time slice 13 after which the signal is lost in noise. The effective mass for this state exhibits good plateau behavior and a good value of the covariance-matrix based χ^2/N_{DF} is obtained when one fits in the time fitting window of $t = 10$–13 (recall, the source is at $t = 3$). Typically, one finds $\chi^2/N_{DF} \approx 1$ and $\chi^2/N_{DF} < 1.5$ throughout. After performing spin and parity projections to extract the $N^{\frac{3}{2}^+}$ state from the interpolating field in Eq. (5), one finds the effective mass plot to be a little noisier, as shown in Fig. 2. There is, however, sufficient information here to extract a mass, and a good value of χ^2/N_{DF} is obtained when one fits in the small time fitting window of $t = 9$–11.

The interpolating field defined in Eq. (5) also has overlap with spin-$\frac{1}{2}$ states of both parities. After performing a spin-$\frac{1}{2}$ projection on the correlation functions, we isolate the $N^{\frac{1}{2}^+}$
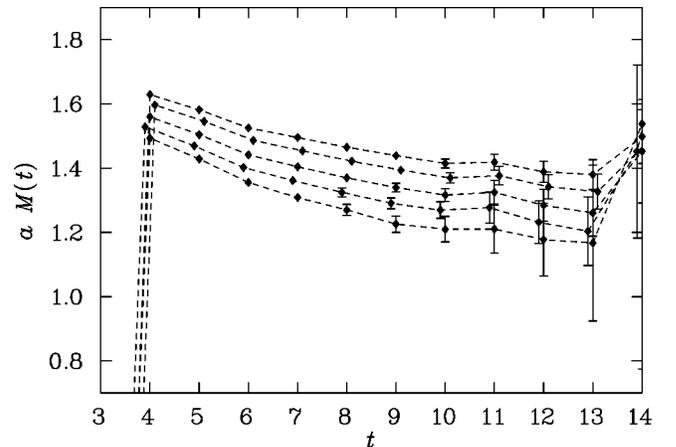
FIG. 1. Effective mass plot for the $N^{\frac{3}{2}^-}$ state using the FLIC action from 392 configurations. The five sets of points correspond to the κ values listed in Table I, with κ increasing from top down.

FIG. 2. As in Fig. 1, but for the $N\frac{3}{2}^{+}$ state.
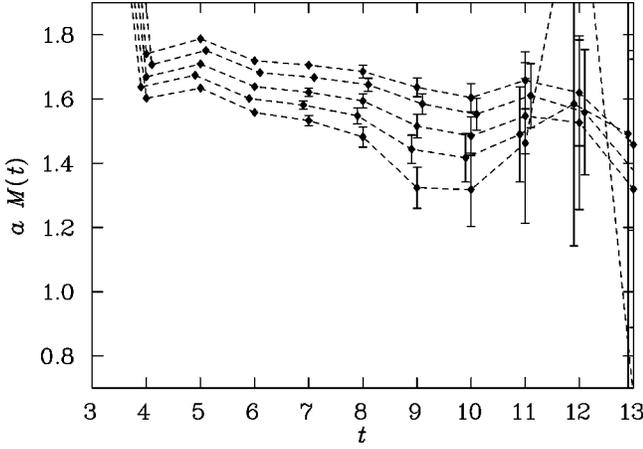
FIG. 4. As in Fig. 1, but for the $N\frac{1}{2}^{-}$ state.

and $N\frac{1}{2}^{-}$ states via parity projection and plot the effective masses in Figs. 3 and 4, respectively. The $N\frac{1}{2}^{+}$ state suffers contamination from excited states as seen by the long Euclidean time evolution required to reach plateau in Fig. 3. A good value of $\chi^2/N_{\rm DF}$ is obtained as long as we fit after time slice 12. For this reason, we use time slices 13–16 to obtain a mass for the $N\frac{1}{2}^{+}$ state. However, for the $N\frac{1}{2}^{-}$ state, a plateau is seen at early Euclidean times and a good value of $\chi^2/N_{\rm DF}$ is obtained on time slices 8–11.

The extracted masses of the $N\frac{3}{2}^{\pm}$ and $N\frac{1}{2}^{\pm}$ states are given in Table I and are displayed in Fig. 5 as a function of m_π^2. Earlier results for the $N\frac{1}{2}^{\pm}$ states using the standard spin-$\frac{1}{2}$ interpolating field [9,13] from Eq. (6) are also shown with open symbols in Fig. 5 for reference. It is encouraging to note the agreement between the spin-projected $\frac{1}{2}^{\pm}$ states obtained from the spin-$\frac{3}{2}$ interpolating field in Eq. (5) and the earlier $\frac{1}{2}^{\pm}$ results from the same gauge field configurations. To study this agreement more accurately, we consider the ratio of effective masses obtained for each jackknife subensemble. This provides us with a correlated ratio and we find the ratio to be one as at the one standard deviation level. We also observe that the $N\frac{3}{2}^{-}$ state has approximately the same
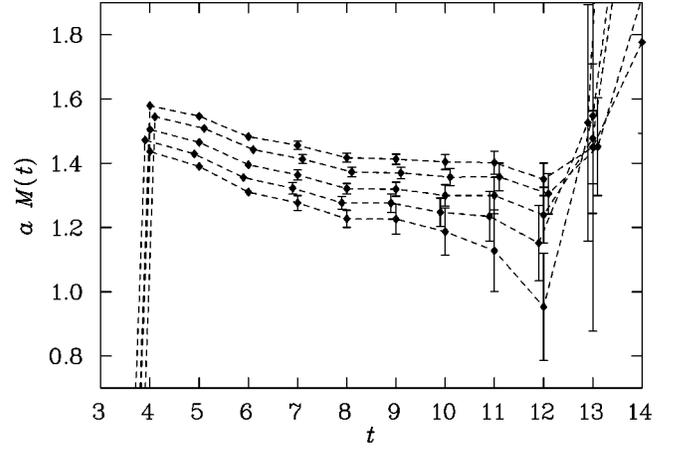
mass as the spin-projected $N\frac{1}{2}^{-}$ state which is consistent with the experimentally observed masses. To study this mass difference more accurately, we again calculate the correlated ratio of effective masses obtained after appropriate spin and parity projections. This ratio is found to be one within one standard deviation. The results for the $N\frac{3}{2}^{-}$ state in Fig. 5 indicate a clear mass splitting between the $N\frac{3}{2}^{+}$ and $N\frac{3}{2}^{-}$ states obtained from the spin-$\frac{3}{2}$ interpolating field, with a mass difference around 300 MeV. This is slightly larger than the experimentally observed mass difference of 200 MeV.

Turning now to the isospin-$\frac{3}{2}$ sector, the effective mass plot for the $\Delta\frac{3}{2}^{+}$ state using the interpolating field given in Eq. (9) is shown in Fig. 6 for the five κ values used. An excellent signal is clearly visible, and a good value of the
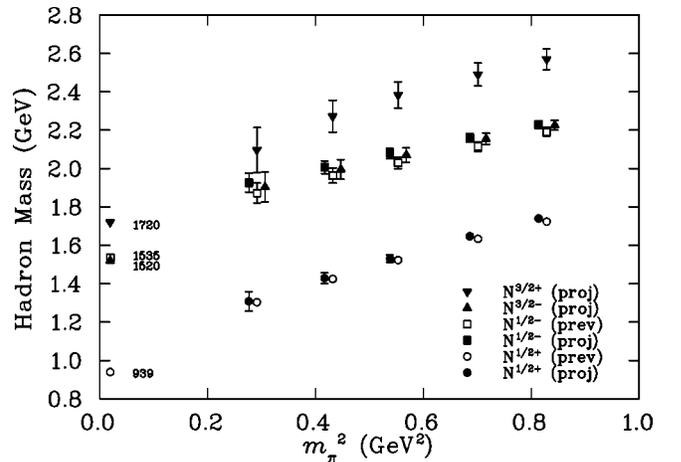
FIG. 5. Masses of the spin projected $N\frac{3}{2}^{-}$ (filled triangles), $N\frac{3}{2}^{+}$ (filled inverted triangles), $N\frac{1}{2}^{+}$ (filled circles), and $N\frac{1}{2}^{-}$ (filled squares) states. For comparison, previous results from the direct calculation of the $N\frac{1}{2}^{+}$ (open circles) and $N\frac{1}{2}^{-}$ (open squares) from Ref. [9] are also shown. The empirical values of the masses of the $N\frac{1}{2}^{+}(939)$, $N\frac{1}{2}^{-}(1535)$, $N\frac{3}{2}^{-}(1520)$ and $N\frac{3}{2}^{+}(1720)$ are shown on the left-hand side at the physical pion mass.

FIG. 3. As in Fig. 1, but for the $N\frac{1}{2}^{+}$ state.
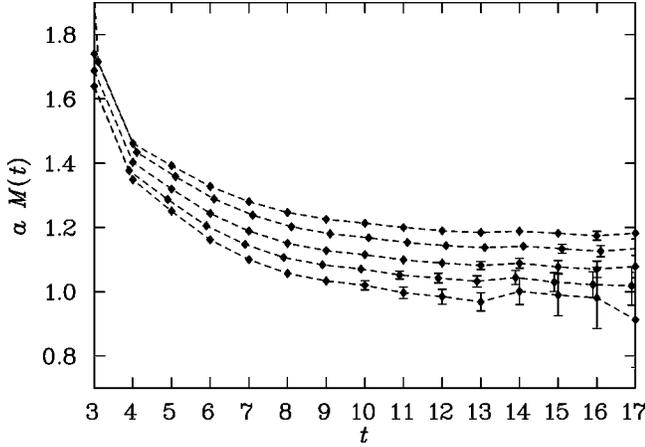
FIG. 6. Effective mass plot for the $\Delta_{\frac{3}{2}}^{+}$ state using the FLIC action with 4 sweeps of smearing at $\alpha=0.7$ from 392 configurations. The five sets of points correspond to the κ values listed in Table II, with κ increasing from top down.

FIG. 7. As in Fig. 6, but for the $\Delta_{\frac{3}{2}}^{-}$ state.

covariance-matrix based χ^2/N_{DF} is obtained by fitting time slices $t=11$–14 following the source at $t=3$. For the effective mass of the negative parity $\Delta_{\frac{3}{2}}^{-}$, shown in Fig. 7, the signal is quite good up to time slice 11–12, but is lost in noise after time slice 12. Time slices $t=9$–12 provide a fitting window with an acceptable value of χ^2/N_{DF}.

The results for the $\Delta_{\frac{3}{2}}^{+}$ and $\Delta_{\frac{3}{2}}^{-}$ masses are shown in Fig. 8 as a function of m_{π}^2. The trend of the $\Delta_{\frac{3}{2}}^{+}$ data points with decreasing m_q is clearly towards the $\Delta(1232)$, although some nonlinearity with m_{π}^2 is expected near the chiral limit [28,29]. The mass of the $\Delta_{\frac{3}{2}}^{-}$ lies some 500 MeV above that of its parity partner, although with somewhat larger errors, as expected from the effective mass plots in Figs. 6 and 7.

After performing a spin projection to extract the $\Delta_{\frac{1}{2}}^{\pm}$ states, a discernible, but noisy, signal is detected. This indicates that the interpolating field in Eq. (9) has only a small overlap with spin-$\frac{1}{2}$ states. However, with 392 configurations we are able to extract a mass for the spin-$\frac{1}{2}$ states at early times, shown in Fig. 8. Here we see the larger error bars associated with the $\Delta_{\frac{1}{2}}^{\pm}$ states. The lowest excitation of the ground state, namely the $\Delta_{\frac{1}{2}}^{-}$, has a mass ~ 350–400 MeV above the $\Delta_{\frac{3}{2}}^{+}$, with the $\Delta_{\frac{3}{2}}^{-}$ possibly appearing heavier. The $\Delta_{\frac{1}{2}}^{+}$ state is found to lie ~ 100–200 MeV above these, although the signal becomes weak at smaller quark masses.

This level ordering is consistent with that observed in the empirical mass spectrum, which is also shown in the figure.

The $N_{\frac{1}{2}}^{-}$ and $\Delta_{\frac{1}{2}}^{-}$ states will decay to $N\pi$ in S wave even in the quenched approximation [30]. For all quark masses considered here, with the possible exception of the lightest quark, this decay channel is closed for the nucleon. While there may be some spectral strength in the decay mode, we are unable to separate it from the resonant spectral strength.

The $N_{\frac{3}{2}}^{+}$ and $\Delta_{\frac{1}{2}}^{+}$ states will decay to $N\pi$ in P wave, while $N_{\frac{3}{2}}^{-}$ and $\Delta_{\frac{3}{2}}^{-}$ states will decay to $N\pi$ in D wave. Since the decay products of each of these states must then have equal and opposite momentum and energy given by

$$E^2 = M^2 + \left(\frac{2\pi}{aL}\right)^2,$$

these states are stable in our calculations.

TABLE II. As in Table I, but for the corresponding $\Delta^{3/2+}, \Delta^{3/2-}, \Delta^{1/2-}$ and $\Delta^{1/2+}$ masses.

κ	$M_{\Delta^{3/2+}}a$	$M_{\Delta^{3/2-}}a$	$M_{\Delta^{1/2+}}a$	$M_{\Delta^{1/2-}}a$
0.1260	1.198(8)	1.469(15)	1.643(109)	1.476(34)
0.1266	1.153(9)	1.429(17)	1.604(107)	1.432(41)
0.1273	1.101(12)	1.385(21)	1.561(106)	1.387(54)
0.1279	1.057(15)	1.353(27)	1.530(109)	1.351(76)
0.1286	1.006(22)	1.331(43)	1.502(119)	1.301(126)
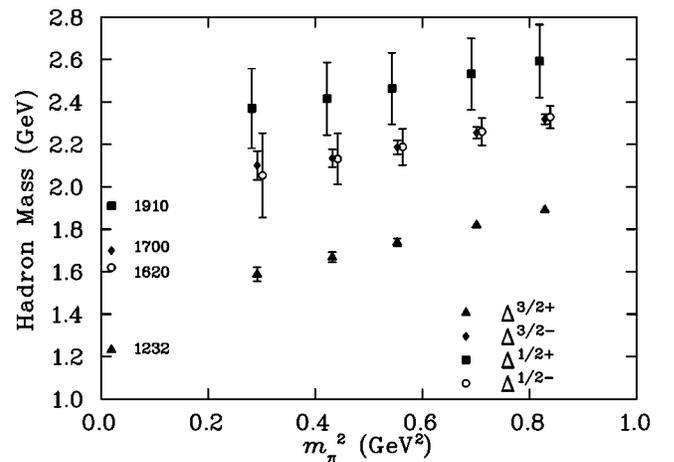
FIG. 8. Masses of the spin-projected $\Delta_{\frac{3}{2}}^{\pm}$ and $\Delta_{\frac{1}{2}}^{\pm}$ resonances. The empirical values of the masses of the $\Delta^{3/2+}(1232)$, $\Delta_{\frac{3}{2}}^{-}(1700)$, $\Delta_{\frac{1}{2}}^{-}(1620)$ and $\Delta_{\frac{1}{2}}^{+}(1910)$ are shown on the left-hand side at the physical pion mass.

IV. CONCLUSION

We have presented the first results for the spectrum of spin-$\frac{3}{2}$ baryons in the isospin-$\frac{1}{2}$ and $\frac{3}{2}$ channels, using a novel fat link irrelevant clover quark action and an $\mathcal{O}(a^2)$ improved gauge action. Clear signals are obtained for both the spin-projected $N\frac{3}{2}^{\pm}$ and $N\frac{1}{2}^{\pm}$ states from a spin-$\frac{3}{2}$ interpolating field. In particular, the $\frac{1}{2}^{\pm}$ states are in good agreement with earlier simulations of the nucleon mass and its parity partner using the standard spin-$\frac{1}{2}$ interpolating field. We find the $N\frac{3}{2}^{-}$ state to lie at a similar energy level to the $N\frac{1}{2}^{-}$, consistent with experiment. We also find a mass difference of ~ 300 MeV between the spin-$\frac{3}{2}$, isospin-$\frac{1}{2}$ parity partners, slightly larger than the experimentally observed difference of 200 MeV.

For isospin-$\frac{3}{2}$ baryons, good agreement is found with earlier calculations for the Δ ground state, and clear mass splittings between the ground state and its parity partner are observed after suitable spin and parity projections. We obtain a signal for the $\Delta\frac{1}{2}^{\pm}$ states and the level ordering is consistent with that observed in the empirical mass spectrum.

It will also be important in future work to consider the excited states in each J^P channel, in particular the lowest "Roper-like" excitation of the $\Delta(1232)$ ground state. Although this will be more challenging [31], it may reveal further insights about the origin of the inter-quark forces and the nature of the confining potential.

[1] N. Isgur, Phys. Rev. D **62**, 054026 (2000).

[2] S. Capstick and W. Roberts, Prog. Part. Nucl. Phys. **45**, S241 (2000).

[3] D.B. Leinweber, Phys. Rev. D **51**, 6383 (1995).

[4] F.X. Lee and D.B. Leinweber, Nucl. Phys. B (Proc. Suppl.) **73**, 258 (1999).

[5] F.X. Lee, Nucl. Phys. B (Proc. Suppl.) **94**, 251 (2001).

[6] D.G. Richards, Nucl. Phys. B (Proc. Suppl.) **94**, 269 (2001); D.G. Richards *et al.*, *ibid.* **100**, 89 (2002).

[7] QCDSF Collaboration, M. Göckeler *et al.*, Phys. Lett. B **532**, 63 (2002).

[8] S. Sasaki, T. Blum, and S. Ohta, Phys. Rev. D **65**, 074503 (2002); S. Sasaki, hep-lat/0110052.

[9] W. Melnitchouk, S. Bilson-Thompson, F.D.R. Bonnet, F.X. Lee, D.B. Leinweber, A.G. Williams, J.M. Zanotti, and J.B. Zhang, Phys. Rev. D **67**, 114506 (2003).

[10] N. Nakajima, H. Matsufuru, Y. Nemoto, and H. Suganuma, hep-lat/0204014.

[11] D.B. Leinweber, A.W. Thomas, K. Tsushima, and S.V. Wright, Phys. Rev. D **64**, 094502 (2001).

[12] V. Burkert *et al.*, Few-Body Syst., Suppl. **11**, 1 (1999).

[13] CSSM Lattice Collaboration, J.M. Zanotti *et al.*, Phys. Rev. D **65**, 074507 (2002); Nucl. Phys. B (Proc. Suppl.) **109**, 101 (2002).

[14] D.B. Leinweber, Ann. Phys. (N.Y.) **198**, 203 (1990).

[15] L.Y. Glozman and D.O. Riska, Phys. Rep. **268**, 263 (1996).

[16] C.L. Schat, J.L. Goity, and N.N. Scoccola, Phys. Rev. Lett. **88**, 102002 (2002); D. Pirjol and C. Schat, Phys. Rev. D **67**, 096009 (2003).

[17] D.B. Leinweber, T. Draper, and R.W. Woloshyn, Phys. Rev. D **46**, 3067 (1992).

[18] F.X. Lee, D.B. Leinweber, L. Zhou, J.M. Zanotti, and S. Choe, Nucl. Phys. B (Proc. Suppl.) **106**, 248 (2002).

[19] D.B. Leinweber *et al.*, nucl-th/0211014. A compiler error rendered some spin-$\frac{3}{2}$ correlation functions negative in this early investigation.

[20] J.M. Zanotti *et al.*, hep-lat/0210043. A compiler error rendered some correlation functions negative in this investigation, interpreted at the time as quenched artifacts associated with the η' meson.

[21] Y. Chung, H.G. Dosch, M. Kremer, and D. Schall, Nucl. Phys. **B197**, 55 (1982).

[22] M. Benmerrouche, R.M. Davidson, and N.C. Mukhopadhyay, Phys. Rev. C **39**, 2339 (1989).

[23] R.G. Edwards, U.M. Heller, and T.R. Klassen, Nucl. Phys. **B517**, 377 (1998).

[24] MILC Collaboration, T. DeGrand, Phys. Rev. D **60**, 094501 (1999).

[25] S. Bilson-Thompson, F.D. Bonnet, D.B. Leinweber, and A.G. Williams, Nucl. Phys. B (Proc. Suppl.) **109**, 116 (2002); S.O. Bilson-Thompson, D.B. Leinweber, and A.G. Williams, Ann. Phys. (N.Y.) **304**, 1 (2003).

[26] S. Gusken, Nucl. Phys. B (Proc. Suppl.) **17**, 361 (1990).

[27] A. Frommer, V. Hannemann, B. Nockel, T. Lippert, and K. Schilling, Int. J. Mod. Phys. C **5**, 1073 (1994).

[28] D.B. Leinweber, A.W. Thomas, K. Tsushima, and S.V. Wright, Phys. Rev. D **61**, 074502 (2000).

[29] R.D. Young, D.B. Leinweber, A.W. Thomas, and S.V. Wright, Phys. Rev. D **66**, 094507 (2002).

[30] J.N. Labrenz and S.R. Sharpe, Phys. Rev. D **54**, 4595 (1996); D.B. Leinweber, hep-lat/0112021.

[31] S. Sasaki, K. Sasaki, T. Hatsuda, and M. Asakawa, hep-lat/0209059.